ELSEVIER

Thin Solid Films 264 (1995) 230–235

thin solid films

Kinetic processes in metal epitaxy studied with variable temperature STM: Ag/Pt(111)

Harald Brune, Holger Röder, Karsten Bromann, Klaus Kern

Institut de Physique Expérimentale, EPF Lausanne, CH-1015 Lausanne, Switzerland

Abstract

Variable-temperature scanning tunneling microscopy has been applied to study kinetic processes involved in epitaxial growth. This paper concentrates on nucleation and aggregation of submonolayer Ag films on a Pt(111) surface. From island density versus temperature data, the activation barrier for Ag adatom diffusion as well as the stability of adsorbed Ag dimers are determined. From the adsorbed aggregate shapes conclusions on Ag perimeter diffusion can be drawn. An anisotropy in edge diffusion leads to dendritic aggregates with the trigonal substrate symmetry. A crossover to randomly ramified fractals is observed upon lowering of the deposition flux.

Keywords: Aggregation; Epitaxy; Kinetics; Nucleation

1. Introduction

The real-space study of the atomic processes involved in thin-film epitaxy has always been challenging. For the submonolayer regime these processes are the diffusion of the film-atoms adsorbed from the vapor phase, the nucleation of stable islands from the two-dimensional gas formed by the mobile adatoms and finally the growth of islands by aggregation of further film atoms. The diffusion of single atoms and their interaction with a step could nicely be followed by means of field ion microscopy at low temperature [1–3]. Nucleation and aggregation, on the other hand, have been studied on a much larger scale so far; either by means of electron [4] or scanning tunneling microscopy (STM) [5–10]. Both techniques, however, were restricted to large-scale observations, i.e. to relatively low island densities and big islands comprising several hundreds of atoms, thus much too large to follow the initial steps of nucleation. This partly resulted from the limited range of temperatures that was accessible in situ. In the present study we show an attempt to close the gap between the observation of single-atom diffusion and that of big islands. We apply STM at variable temperature to study the atomic processes involved in the initial phases of nucleation, the transition from nucleation to growth and finally the aggregation of a metal film.

2. Experiment

The experiments were performed in ultrahigh vacuum with standard facilities for sample preparation and film evaporation. The Pt(111) crystal was cleaned by repeated cycles of Ar ion bombardment (650 eV) at 830 K, annealing in oxygen atmosphere (880 K, 1×10^{-7} mbar) and subsequent flash to 1200 K. The Ag (purity 99.995%) aggregates were grown by vapor-phase epitaxy with a molecular beam epitaxy (MBE) Knudsen cell at a background pressure better than 2×10^{-10} mbar.

The variable-temperature scanning tunneling microscope is a home-built instrument which allows for measurements at temperatures ranging from 25 K to 800 K (see Fig. 1(a)). It is based on the "Beetle"-type STM [11], where thermal drift is, to first order, compensated by the fact that it stands on piezo-legs which have equal thermal expansion rates as the single-tube scanner to which the tip is mounted. The sample is hat-shaped and it is clamped on its brim between a small copper disk and a molybdenum ring which provides the ramps for the inertial approach [12]. For cooling, the Cu disk is connected to a liquid He-flux cryostat via a soft copper braid (ϕ, 4 mm; length, 50 mm), which is untwisted into several single cords. Heating is done either by radiation or by electron bombardment from a filament located behind

SSDI 0040-6090(94)05821-0

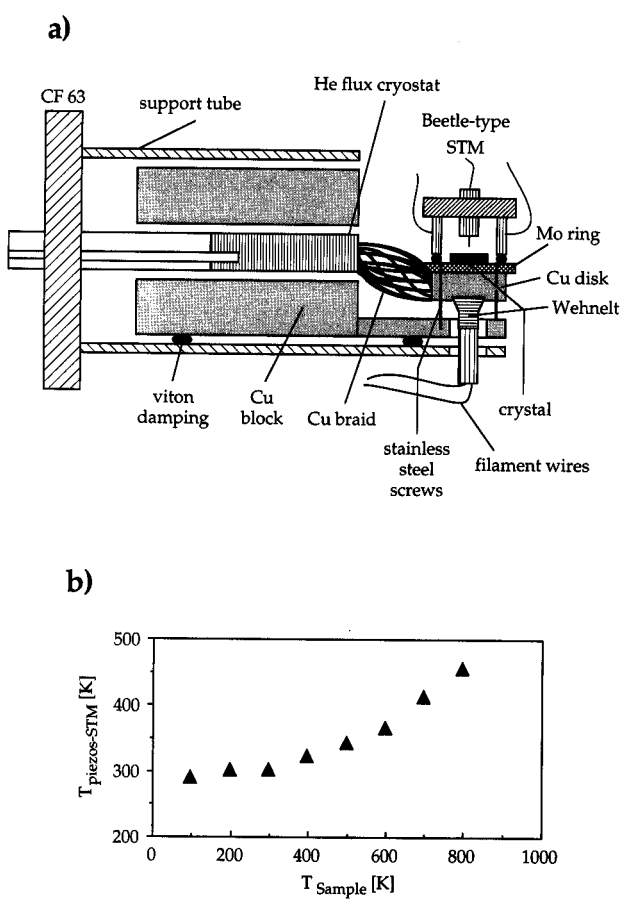

Fig. 1. Variable-temperature STM (25 K–800 K). (a) Side-view on the cryogenic sample holder. It is mounted onto a CF63 rotary flange in order to have free access to LEED, AES, the sputter gun and the Knudsen cell when the STM is lifted. (b) Plot of the temperature measured at the piezoceramics of the "Beetle"-type STM as a function of sample temperature. The temperatures are equilibrium values obtained after 1 h.

the sample. This small sample holder is rigidly mounted onto a big cylindrical copper block which itself resides on viton spacers inside a steel tube [13]. The viton serves to damp external high-frequency vibrations. The mechanical vertical stability of the STM is 0.1 Å. No detectable change in stability is observed when the He flux is turned on, i.e. vibrations caused by the He flux at the cryostat are effectively decoupled from the sample by means of the soft Cu braid and the big Cu block where the sample is attached.

The desired temperature is adjusted upon regulation of the filament current by a commercial PID controller. The temperature is measured by a thermocouple (Ni–CrNI; ϕ, 0.1 mm); its wires are spot-welded separately onto the brim of the crystal in order to ensure that the thermocouple "hot junction" is on the crystal [14]. The temperature stability is 0.1 K, which is sufficient to reduce thermal drift in STM images below 5 nm min^{-1}. From nucleation studies at low temperatures [15] it is inferred that the absolute value measured for the temperature can be reproduced within 1 K between different experiments. In order to have quick access to different temperatures with STM, i.e. to have small equilibration times of about 10 min, we took care to cool or heat only the sample (together with its small holder), i.e. for low temperatures the big Cu block as well as the STM basically stay at room temperature. For the Cu block this is achieved by the use of thin stainless steel screws to mount the sample holder [14].

Fig. 1(b) shows how the temperature of the STM's piezos changes with sample temperature. At low temperatures, where the radiative energy transfer is small, the piezo-ceramics remain to a good approximation at room temperature (the thermal contact between piezos and the Mo-ring via stainless steel spheres is sufficiently bad). For sample temperatures above room temperature radiative heating steadily increases the temperature of the piezoceramics. In order to avoid their depolarization, we chose the upper limit for the sample temperature at 800 K where the piezos stay at 450 K.

For the STM images shown here ($-0.5\ V \leq V_t \leq -1.5\ V$, $10\ nA \leq I_t \leq 3.0\ nA$), the derivative $\partial z/\partial x$ of the lines of constant tunnel current has been recorded. They therefore represent the surface as it appears when illuminated from the left. Island densities are given in islands per Pt substrate atom, i.e. in monolayers (ML). They were corrected for lateral drift.

3. Results and discussion

When Ag is deposited onto the Pt(111) surface held at sufficiently low temperature, the Ag atoms rest immobile on the lattice site of their impact (or at least close to it, if transient mobility was involved [16–18]). Because diffusion is frozen in, we expect to predominantly see single adsorbed Ag atoms. This is shown in Fig. 2, where 0.10 ML of Ag have been deposited at 35 K. The Ag nuclei are imaged as protruding (2–3 Å) dots. Their mean size, as inferred from coverage and island density, is 1.2 ± 0.3 atoms, thus the majority represents single Ag atoms. The lateral extension of the protrusions in Fig. 2 is 4–7 A, which is comparable with the imaging size of Fe atoms adsorbed on Pt(111) [19].

The nucleation of islands sets in when diffusion of Ag adatoms becomes activated. The development of the island density and size with increasing coverage has been monitored at 75 K. Four STM images are shown in Figs. 3(a)–3(d) in order to illustrate the transition from the initial steps of nucleation to island growth. In Figs. 3(a) and 3(b), it is seen that on the average, the islands are dimers (mean size 2.4 ± 0.4 atoms and 2.6 ± 0.5 atoms for Figs. 3(a) and 3(b),

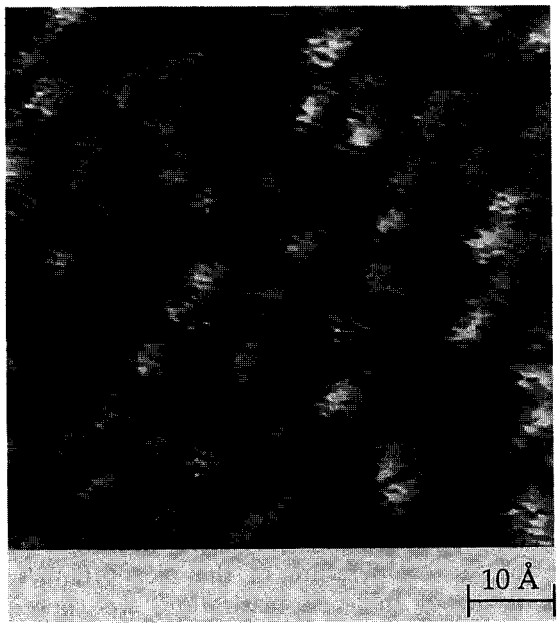

Fig. 2. STM image taken after deposition of coverage $\Theta = 0.10$ ML Ag at $T = 35$ K. The average island side is $n = 1.2 \pm 0.3$ atoms (island density $\rho = 0.083$ ML, 68 Å × 68 Å, $R = 1.1 \times 10^{-3}$ ML s^{-1}).

respectively). These dimers are observed to be immobile and stable in consecutive STM images. The fact that the density of nuclei increases almost linearly with coverage from Fig. 3(a) to Fig. 3(b) (the mean island size remains constant), means that we are in the coverage regime of pure nucleation. In this regime, diffusing Ag atoms find, with a higher probability, a second mobile partner to create a new nucleus than to attach to an existing nucleus. Of course, above a certain density of nuclei, diffusing Ag atoms attach with comparable probability to an existing nucleus, rather than to create a new nucleus. This transition from nucleation to growth is seen in Fig. 3(c). The coverage was increased by a factor of five with respect to Fig. 3(b), which resulted in an increase in density by a factor of only two accompanied by an increase in the average island size to 6.4 ± 1.1 atoms. Further increase of the coverage by a factor of two leads to exclusive island growth (11.9 ± 2.0 atoms per island (see Fig. 3(d)). The island density has reached its saturation value, from where on diffusing Ag adatoms are solely captured at existing islands rather than meet each other.

The saturation island density therefore marks the mean free path of a diffusing Ag atom, in other words its diffusion rate relative to the applied deposition flux. From an Arrhenius plot of the saturation island density versus temperature, the diffusion barrier for Ag adatoms has been determined as 157 ± 10 meV [20] upon application of mean-field nucleation theory [4]. An important ingredient in this analysis is the size of the critical nucleus. From the images shown in Fig. 3 we see that dimers are stable at 75 K, thus the critical nucleus is a single atom. In fact, annealing [21] and nucleation experiments (such as flux dependency of saturation island density [20]) show that this is valid up to 110 K. At higher temperatures, however, the saturation island densities show a marked deviation from the dimer analysis. This is due to dimer dissociation on the time scale of deposition. The threshold temperature for dissociation as well as the development of island density for $T > 110$ K lead to an estimate for the dissociation barrier for Ag_2 adsorbed on Pt(111) of 320 ± 20 meV [20].

As can be seen from Fig. 3(d), island growth leads to branching of the islands. This is caused by the low perimeter mobility for attaching atoms [22]. Note that this branching is not observed in Fig. 3(c), which implies that it proceeds only if the islands have reached a certain size (7 atoms). Note further that the branching is anisotropic, it occurs exclusively in three crystallographically equivalent directions. Thus Y shapes are formed with arms 120° apart from each other and only one orientation of these Y shapes is found [23].

Bigger aggregates, which have been grown upon deposition of 0.12 ML Ag at 130 K, are shown in Fig. 4(a). A nice dendritic pattern is observed. It is characterized by three axes of preferred growth which are oriented along the crystallographic $\langle 11\bar{2} \rangle$ directions of the substrate. They correspond to those of the branches of the Y shapes in Fig. 3(d).

The nature of this growth anisotropy is linked to the trigonal symmetry of the Pt(111) surface. A densely packed cluster on an fcc (111) surface is bound by two types of edges with atomically different structure (A and B edges). A edges are {100} facets whereas B edges are {111} facets (see Fig. 5, left-hand side). This microscopic difference is partly reflected in a different activation barrier for perimeter diffusion. For Ag/Pt(111) we find the direction of preferred growth to be perpendicular to the A edges [23]. Because Ag atoms arrive at random at each edge orientation, the fact that growth predominantly occurs in the three directions perpendicular to the A steps must invoke perimeter diffusion along the B steps, whereas diffusion along the A steps is frozen in. Thus the latter must have a higher activation barrier (this anisotropy is found from 60 K to 130 K). Therefore only one orientation of Y shapes occurs (right-hand side of Fig. 5) and larger aggregates grow dendritically with the three axes of preferred growth perpendicular to the A steps.

Interestingly this anisotropy is only realized for high deposition flux. If the flux is lowered by two orders of magnitude, a drastic change in the aggregates' pattern is observed, and randomly ramified fractals result.

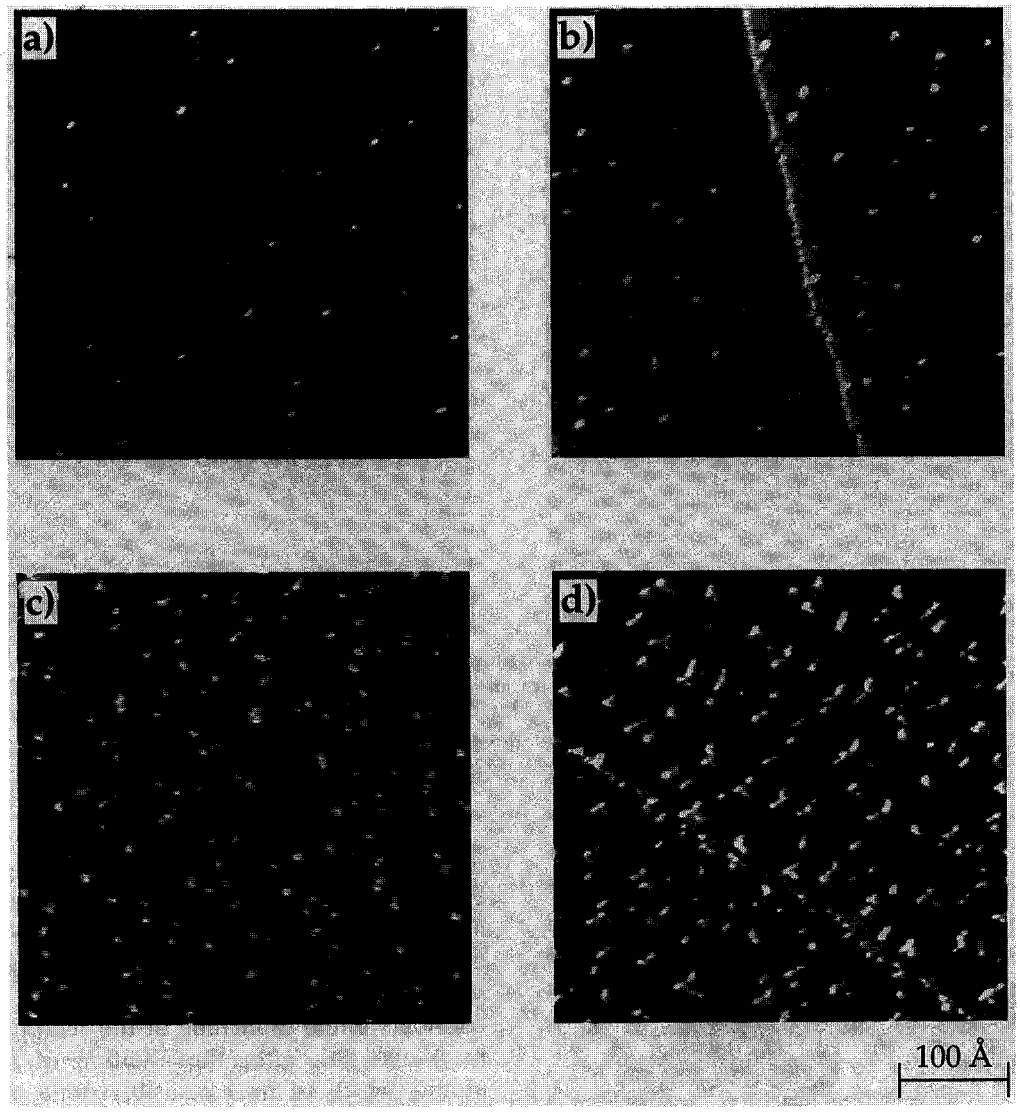

Fig. 3. (a)–(d) Four STM images showing the evolution of the island shape and density as a function of coverage at 75 K: (a) coverage, $\Theta = 0.24\%$, $\rho = 0.10\%$; (b) $\Theta = 0.60\%$, $\rho = 0.23\%$; (c) $\Theta = 3.0\%$, $\rho = 0.46\%$; (d) $\Theta = 6.0\%$, $\rho = 0.50\%$ of 1 ML. (a)–(d) 420 Å × 420 Å.

This is shown in Fig. 4(b), where the same coverage of Ag has been deposited with low flux onto the Pt(111) substrate held at 110 K. The branches of the clusters frequently alter their direction of growth and thus show no more long-range correlation with the trigonal substrate symmetry. The shape of these Ag aggregates is very similar to that of fractal aggregates simulated with the classical DLA computer codes either performed off-lattice (no anisotropy) [24, 25] or on-lattice with noise-dominating lattice anistropy [24, 26]. The insets in Figs. 4(a) and 4(c) demonstrate that the transition from dendrites to fractals is solely linked to the flux and largely independent from temperature. Randomly ramified fractals result for the low flux applied at 130 K (inset Fig. 4(a)) and dendrites result for deposition with the high flux at 110 K (inset Fig. 4(b)).

The observation of such a transition in shape linked to the growth speed is in full agreement with earlier "macroscopic" studies of pattern formation. Increasing the growth speed (Zn^{2+} concentration and voltage) in electrochemical deposition resulted in transition from fractal to dendritic patterns [27, 28]. In the propagation of a low viscous medium into a high viscous one in a Hele–Shaw cell [29] above certain propagation speed, viscous fingering occurs (Saffman–Taylor instability [30]). The dynamics is dominated by tip bifurcations which lead to randomly branched structures. When anisotropy is introduced into these systems, either by scratching a lattice into one of the glass plates of the Hele–Shaw cell [31, 32], or by use of a liquid crystal as a high viscous medium [33], a transition from randomly ramified to dendritic patterns is found. This transition takes place upon in-

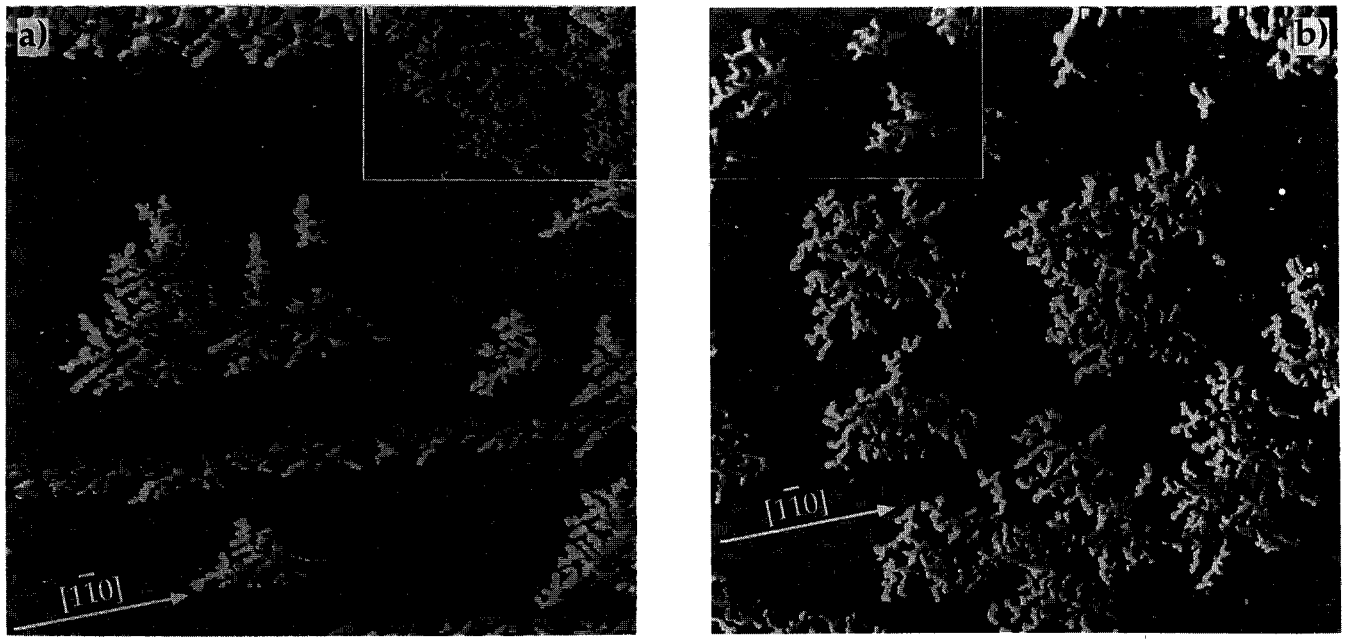

Fig. 4. Dendritic and fractal Ag aggregates on Pt(111). (a) STM image showing the dendritic shape of the Ag aggregates grown at 130 K with a flux of $R = 1.1 \times 10^{-3}$ ML s^{-1} (1200 Å × 1200 Å, $\Theta = 0.12$ ML); inset, transition from dendritic to fractal growth at 130 K upon lowering of the deposition flux by two orders of magnitude (830 Å × 520 Å, $\Theta = 0.12$ ML, $R = 1.6 \times 10^{-5}$ ML s^{-1}). (b) STM image sowing fractal (randomly ramified) Ag aggregates grown on Pt(111) at 110 K and a deposition flux of 1.6×10^{-5} ML s^{-1} (1200 Å × 1200 Å, $\Theta = 0.12$ ML); inset, small dendritic islands obtained at 110 K and high flux (530 Å × 330 Å, $\Theta = 0.12$ ML, $R = 1.1 \times 10^{-3}$ ML s^{-1}).

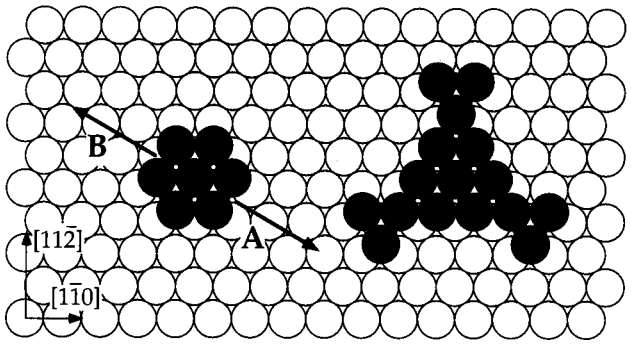

Fig. 5. Different microscopic structures of dense steps on fcc (111) surfaces leads to anisotropy in edge diffusion and thus to preferred growth directions.

crease of the expansion rate, which, again is in accordance with the results presented above. Therefore the transition in island shape observed here for the diffusion-limited aggregation of Ag on a Pt(111) surface is very likely to be a general phenomenon. The systems from electrochemistry and fluid dynamics, cited above, as well as Ag/Pt(111) all have in common the fact that anisotropy and randomness are both present, depending on the growth rate the first or the second dominate.

The atomic-scale mechanism which explains the dominance of randomness over anisotropy for low growth speeds, leading to random ramification, can be analyzed for the present system Ag/Pt(111). The anisotropy in edge diffusion is necessary but not sufficient to grow the branches of the Y shapes. If one considers initial branching of the seed particle (heptamer) one has, after the addition of the first three atoms (which is most plausibly done at the A steps where diffusion is frozen), a Ag_{10} aggregate which is exclusively bound by B steps. In order to grow a stable expansion in the A direction, as observed, two diffusing perimeter atoms have to meet each other at one of the aggregate's corners. Such an event, however, is more probable the more diffusing atoms are present at a time at the island perimeter. Their quantity, on the other hand, is directly related to the impinging rate onto the island perimeter, which itself is proportional to the deposition flux. At the high flux used in Fig. 4(a) there are on average 100 atoms arriving per second at the aggregate's perimeter, whereas there is only one per second at the low flux in Fig. 4(b). Therefore the probability for two atoms meeting at a corner is higher at increased flux, and, due to faster migration along the B steps, also much more probable at those corners that point in the A direction. Thus trigonal dendrites (or Y shapes) with growth perpendicular to the A steps are formed for high flux. At low flux, on the other hand, the interaction of two diffusing particles at the aggregates perimeter is less prob-

able and predominantly single non-interacting mobile atoms are present at the step. Therefore anisotropy loses more of its importance in favour of noise and the aggregate grows randomly.

4. Conclusions

In summary, we have shown that the application of variable-temperature STM to study epitaxy opens up the possibility of observing the very initial steps of nucleation and to follow aggregation. The temperature dependence of island density was analyzed to extract activation barriers for Ag-terrace diffusion as well as Ag-dimer dissociation. From the shape of the aggregates, an anisotropy in edge diffusion with easier diffusion along the B edges and growth perpendicular to the A edges has been inferred. This anisotropy leads to dendritic growth at high deposition flux. At low growth rates, a transition to randomly ramified aggregates is observed. The mechanism responsible for the dominance of randomness over anisotropy at low growth rates has been discussed.

References

[1] G. Ehrlich, *Surf. Sci.*, *246* (1991) 1.
[2] S.C. Wang and G. Ehrlich, *Phys. Rev. Lett.*, *70* (1993) 41.
[3] S.C. Wang and G. Ehrlich, *Phys. Rev. Lett.*, *71* (1993) 4174.
[4] J.A. Venables, G.D.T. Spiller and M. Hanbücken, *Rep. Prog. Phys.*, *47* (1984) 399.
[5] J.A. Stroscio, D.T. Pierce and R.A. Dragoset, *Phys. Rev. Lett.*, *70* (1993) 3615.
[6] J.A. Stroscio and D.T. Pierce, *Phys. Rev. B*, *49* (1994) 8522.
[7] C. Günther, S. Güntehr, E. Kopatzki, R.Q. Hwang, J. Schröder, J. Vrijmoeth and R.J. Behm, *Ber. Bunsenges. Phys. Chem.*, *97* (1993) 522.
[8] S. Günther, E. Kopatzki, M.C. Bartelt, J.W. Evans and R.J. Behm, *Phys. Rev. Lett.*, *73* (1994) 553.
[9] T. Michely, M. Hohage, M. Bott and G. Comsa, *Phys. Rev. Lett.*, *70* (1993) 3943.
[10] P.A. Bennett, S.A. Parikh and D.G. Cahill, *J. Vac. Sci. Technol. A*, *11* (1993) 1680.
[11] K. Besocke, *Surf. Sci.*, *181* (1987) 145.
[12] J. Frohn, J.F. Wolf, K. Besocke and M. Teske, *Rev. Sci. Instrum.*, *60* (1989) 1200.
[13] T. Michely and G. Comsa, *Surf. Sci.*, *256* (1991) 217.
[14] R. David, K. Kern, P. Zeppenfeld and G. Comsa, *Rev. Sci. Instrum.*, *57* (1986) 2771.
[15] R. Stumpf and M. Scheffler, *Phys. Rev. Lett.*, *72* (1994) 254.
[16] T. Gurney, F. Hutchinson and R.D. Young, *J. Chem. Phys.*, *42* (1965) 3939.
[17] R.D. Young and D.S. Schubert, *J. Chem. Phys.*, *42* (1965) 3943.
[18] J.W. Evans, D.E. Sanders, P.A. Thiel and A.E. DePristo, *Phys. Rev. B*, *41* (1990) 5410.
[19] M.F. Crommie, C.P. Lutz and D.M. Eigler, *Phys. Rev. B*, *48* (1993) 2851.
[20] H. Brune, H. Röder, C. Boragno and K. Kern, *Phys. Rev. Lett.*, *73* (1994) 1955.
[21] H. Röder, E. Hahn, H. Brune, J.P. Bucher and K. Kern, *Nature*, *366* (1993) 141.
[22] T.A. Witten and L.M. Sander, *Phys. Rev. B*, *27* (1983) 5686.
[23] H. Brune, C. Romainczyk, H. Röder and K. Kern, *Nature*, *369* (1994) 469.
[24] P. Meakin, *Phys. Rev. A*, *27* (1983) 1495.
[25] J.P. Eckmann, P. Meakin, I. Procaccia and R. Zeitak, *Phys. Rev. Lett.*, *65* (1990) 52.
[26] T.A. Witten and L.M. Sander, *Phys. Rev. Lett.*, *47* (1981) 1400.
[27] Y. Sawada, A. Dougherty and J.P. Gollub, *Phys. Rev. Lett.*, *56* (1986) 1260.
[28] D. Grier, E. Ben-Jacob, R. Clarke and L.M. Sander, *Phys. Rev. Lett.*, *56* (1986) 1264.
[29] H. Brune and K. Kern, *Phys. Low-Dim. Struct.*, *1* (1994) 67.
[30] H. Brune, H. Röder, C. Romainczyk, C. Boragno and K. Kern, *Appl. Phys. A*, *60* (1995) 167.
[31] E. Ben-Jacob, R. Godbey, N.D. Goldenfeld, J. Koplik, H. Levine, T. Mueller and L.M. Sander, *Phys. Rev. Lett.*, *55* (1985) 1315.
[32] V. Horváth, T. Vicsek and J. Kertész, *Phys. Rev. A*, *35* (1987) 2353.
[33] A. Buka, J. Kertész and T. Vicsek, *Nature*, *323* (1986) 424.